# Radial excitations in the analysis of $\phi$-$\omega$ and $\eta$-$\eta'$ mixing

Bo Huang, Xiang-Dong Li, and C. M. Shakin*
*Department of Physics and Center for Nuclear Theory, Brooklyn College of the City University of New York, Brooklyn, New York 11210*

(Received 3 December 1997; revised manuscript received 29 July 1998)

We continue our studies of a unified model of meson structure that makes use of a Nambu–Jona-Lasinio (NJL) model that has been generalized to include a relativistic model of confinement. (We use Lorentz-vector confinement, so that the Lagrangian exhibits chiral symmetry in the absence of a quark mass matrix.) Here we study $\phi$-$\omega$ and $\eta$-$\eta'$ mixing. The latter study requires that we include the 't Hooft interaction in our model. We study states of $\bar{q}q$ structure for energies $P^2 \leqslant 3$ GeV$^2$. The coupled $\phi$-$\omega$ system exhibits ideal mixing, such that the $\omega$ and its radially-excited states have no strange quark content, while the $\phi$ states are pure $s\bar{s}$ configurations. In the case of $\eta$-$\eta'$ mixing, the 't Hooft interaction gives rise to a $P^2$-dependent mixing angle $\theta_P(P^2)$. At the energy of the $\eta(547)$, $\theta_P(m_\eta^2) = -11.5°$, while at the energy of the $\eta'(958)$, we have $\theta_P(m_{\eta'}^2) = -36.3°$, if we take singlet-octet mixing into account. We obtain a satisfactory fit to experimental values for energies of the radially-excited states of the $\phi$-$\omega$ system, as well as for the decay constants of the $\omega(782)$ and the $\phi(1020)$. The predictions for the radially-excited $\bar{q}q$ states of the $\eta$ and $\eta'$ are not as good, if those states are to be identified as the $\eta(1295)$ and $\eta(1440)$. [However, we do find a state at 1370 MeV which is halfway between the $\eta(1295)$ and $\eta(1440)$. That suggests the presence of a non-$q\bar{q}$ state that could mix with our state at 1370 MeV to produce the two states at 1295 and 1440 MeV. The state at 1370 MeV is found to have very little $s\bar{s}$ component. Thus one might suggest a correspondence with the $\omega(1420)$, which is also a $2S$ state.] Further work is needed to understand the spectrum of the $\eta$-$\eta'$ system of states above $P^2 = 1.0$ GeV$^2$, where one may encounter low-energy pseudoscalar glueball states. We extend our work on singlet-octet mixing to include pseudoscalar-axialvector mixing. In that case there are two mixing angles and two coupling constants to be calculated. It is found that the spectrum obtained with singlet-octet mixing is largely unchanged upon addition of pseudoscalar-axialvector mixing, if a small value for the strength of the 't Hooft interaction is used. A small 't Hooft interaction implies ideal mixing for the $\eta$-$\eta'$ pair. It remains to be seen if the wave functions in this case are consistent with experimental decay rates. [S0556-2813(98)04412-4]

PACS number(s): 24.85.+p, 12.39.Ki, 12.40.Yx, 14.40.Aq

## I. INTRODUCTION

In a number of papers, we have been studying a generalized Nambu–Jona-Lasinio model that includes a relativistic model of confinement [1–4]. In general, the inclusion of confinement will lead to a momentum-dependent quark mass, when we solve the "gap" equation. That feature was taken into account in an earlier work [2], where we carried out a calculation in Euclidean space and showed that the Goldstone theorem was satisfied. In the present work, and in most of our earlier work, we use constant values of the masses of the up, down, strange, charm and bottom quarks. With that approximation, we are able to obtain a good fit to the observed meson spectra [5].

One good feature of our model is that the calculational procedure is the same for all mesons that are of $q\bar{q}$ structure. In this work we apply our model to the calculation of the masses of $\eta$ and vector mesons in the energy region $P^2 \leqslant 3.0$ GeV$^2$. One of our goals is to demonstrate that our (unified) model of meson spectra works well for a large number of mesons of quite different mass values.

The organization of our work is as follows. In Sec. II, we describe the Lagrangian of our model which includes a relativistic model of confinement and the 't Hooft interaction. That interaction plays an important role in understanding the properties of the $\eta$ and $\eta'$ mesons [6,7]. In the present work we study whether the 't Hooft interaction can yield a good account of the radially-excited states of the $\eta$ and $\eta'$ mesons. In Sec. III we describe how the energies of the $\phi$ and $\omega$ mesons are obtained, while in Sec. IV we consider $\eta$-$\eta'$ mixing. In Sec. V we present the results of our calculations of the properties $\phi$ and $\omega$ mesons of $\eta$-$\eta'$ mixing. Finally, Sec. VI contains some further discussion and conclusions.

## II. A GENERALIZED NAMBU–JONA-LASINIO MODEL

The Lagrangian we consider in this work is based on the SU(3)-flavor version of the NJL model [6,7]

$$\begin{aligned}\mathcal{L} = {} & \bar{q}(i\not{\partial} - m^0)q + \frac{G_1}{2}\sum_{i=0}^{8}[(\bar{q}\lambda^i q)^2 + (\bar{q}i\gamma_5\lambda^i q)^2] \\ & + 2H\{\det[\bar{q}(1+\gamma_5)q] + \det[\bar{q}(1-\gamma_5)q]\} \\ & - \frac{G_2}{2}\sum_{i=0}^{8}[(\bar{q}\gamma^\mu\lambda^i q)^2 + (\bar{q}\gamma^\mu\gamma_5\lambda^i q)^2] + \mathcal{L}_{\text{conf}},\end{aligned} \tag{2.1}$$

where $m^0 = \text{diag}(m_u^0, m_d^0, m_s^0)$ and the $\lambda^i$ $(i=1,...,8)$ are the Gell-Mann matrices. Here $\lambda^0 = (2/3)^{1/2} I$, with $I$ being the unit matrix in flavor space. The term proportional to $H$ is the 't Hooft interaction and $\mathcal{L}_{\text{conf}}$ denotes our model of confine-

*Electronic address: CASBC@CUNYVM.CUNY.EDU

 

ment. In Eq. (2.1) we have used the notation of Ref. [8] to facilitate comparison with that work. We use Lorentz-vector confinement with

$$\mathcal{L}_{\rm conf}=\int d^4y\overline{q}(x)\gamma^\mu q(x)V^c(x-y)\overline{q}(y)\gamma_\mu q(y). \tag{2.2}$$

Here, $V^c(r)=\kappa r\,\exp(-\mu r)$ where $\kappa$ is the "string tension" and $\mu$ is a small parameter used to soften the singularities of the Fourier transform of $V^c(r)$. The Fourier transform of $V^c(r)$ is then

$$V^c(\vec{k}-\vec{k}\,')=-8\pi\kappa\left[\frac{1}{[(\vec{k}-\vec{k}\,')^2+\mu^2]^2}-\frac{4\mu^2}{[(\vec{k}-\vec{k}\,')^2+\mu^2]^3}\right], \tag{2.3}$$

In this work, we study the $\omega$, $\phi$, $\eta$, and $\eta'$ mesons and their radially excited states. In an earlier work, we studied the spectrum of the $\omega$, $J/\psi$, and $Y$ mesons and their radially excited states [5]. Good fits were obtained to the fourteen states to be found in the data tables. Our work on the $\omega$ used $m_d=m_u=0.364$ GeV, $\mu=0.020$ GeV, and $\kappa=0.0575\ \mathrm{GeV}^2$. (Since we are using Lorentz-vector confinement, this value of $\kappa$ is not directly related to the value of $\kappa$ used in Lorentz-scalar confinement for massive quark systems.) We maintain these values of the parameters and study the $\phi$ meson here. That study is used to fix $G_2$ of Eq. (2.1) at $G_2=6.25\ \mathrm{GeV}^{-2}$ and the constituent mass of the strange quark at $m_s=0.565$ GeV. In this manner, we fix several of the parameters of the model.

### III. VECTOR MESONS: $\phi$-$\omega$ MIXING

Our study requires that we introduce a vacuum polarization tensor [5,9]

$$-i\hat{J}^{\mu\nu}(P)=(-1)n_c\int\frac{d^4k}{(2\pi)^4}\,\mathrm{Tr}[iS(P/2+k)\Gamma^\mu(P,k)\times iS(-P/2+k)\hat{\gamma}^\nu], \tag{3.1}$$

where $S(P)=[\not{P}-m_q+i\epsilon]^{-1}$. (See Fig. 1 and Fig. 2.) Here $n_c=3$ is the number of colors and $\Gamma^\mu(P,k)$ represents a vertex function that sums a "ladder" of confining interactions. [See Eq. (A2) for the definition of $\hat{\gamma}^\nu$ and see Appendixes A and B for details concerning the calculation of $\hat{J}^{\mu\nu}(P)$ and $\Gamma^\mu(P,k)$.] In the case of the up quark, we write

$$\hat{J}_u^{\mu\nu}(P)=-\tilde{g}^{\mu\nu}(P)\hat{J}_u^V(P^2), \tag{3.2}$$

with $\tilde{g}^{\mu\nu}=g^{\mu\nu}-P^\mu P^\nu/P^2$. A similar definition is made for $\hat{J}_d^V(P^2)$ and $\hat{J}_s^V(P^2)$. (See Fig. 3 and Fig. 4.)

Since the $\phi$-$\omega$ system exhibits ideal mixing, we may obtain the energy of the $\omega$ and its radially excited states by solving

$$1-G_VJ_\omega(P^2)=0, \tag{3.3}$$

when $G_V=2G_2$ and $J_\omega(P^2)=2\hat{J}_u^V(P^2)$. (As we will see, a good fit to the $\omega$ and its radially excited states is found for $G_V=12.5\ \mathrm{GeV}^{-2}$, $m_u=0.364$ GeV, and $\kappa=0.0575\ \mathrm{GeV}^2$.)

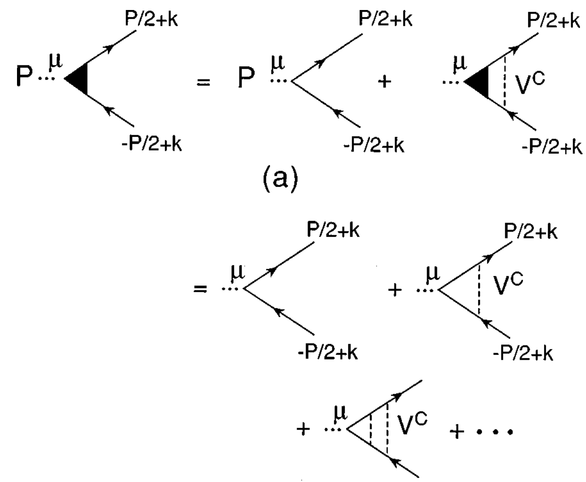


FIG. 1. (a) The equation for the vertex operators, $\Gamma^\mu(P,k)$, is shown. The vertex is represented by the filled triangular area and the dashed line represents the confining interaction. (See Fig. 2.) (b) A perturbation expansion is shown for the equation in (a). We see that the vertex serves to sum a "ladder" of confining interactions.

In a similar fashion, we may find the energy of the $\phi$ and its radially excited states by solving

$$1-G_VJ_\phi(P^2)=0, \tag{3.4}$$

with $J_\phi(P^2)=2\hat{J}_s^V(P^2)$. That analysis leads us to choose $m_s=0.565$ GeV.

Note that for each state found from the solution of Eqs. (3.3) and (3.4) we may define a meson-quark coupling constant

$$g_{\omega qq}^2=\left[\frac{\partial J_\omega(P^2)}{\partial P^2}\bigg|_{P^2=m_\omega^2}\right]^{-1} \tag{3.5}$$

and

$$g_{\phi qq}^2=\left[\frac{\partial J_\phi(P^2)}{\partial P^2}\bigg|_{P^2=m_\phi^2}\right]^{-1}. \tag{3.6}$$

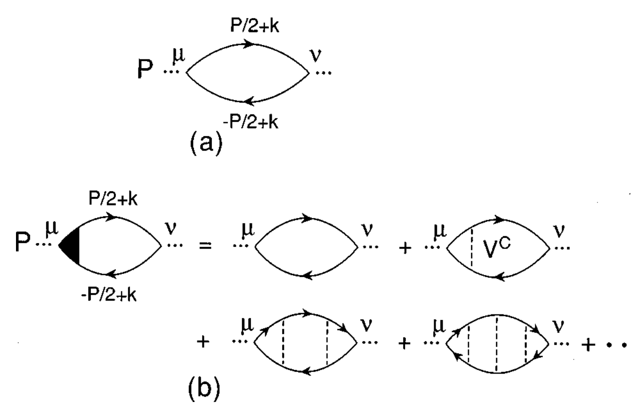


FIG. 2. (a) The diagram shows the basic vacuum polarization diagram of the NJL model that is evaluated in the calculation of the tensor $J^{\mu\nu}(P^2)$. (b) The diagram serves to define the tensor $\hat{J}^{\mu\nu}(P^2)$. The shaded triangular area represents the confining vertex of Fig. 1. The right-hand side of the figure shows a perturbative expansion for $\hat{J}^{\mu\nu}(P^2)$.

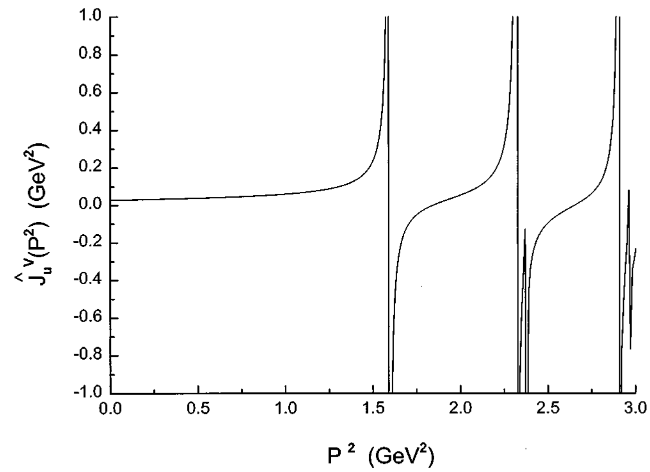


FIG. 3. The figure shows $\hat{J}_u^V(P^2)$ for the parameters $m_u = 0.364$ GeV, $\kappa = 0.0575$ GeV$^2$, $\mu = 0.020$ GeV, and $\Lambda_3 = 0.622$ GeV. The singularities, whose position are given by the vertical lines, are at the energies of the bound states of the confining potential. The peaked structures to the right of the second and third vertical lines indicated the positions of states of angular momentum $L=2$ in the confining potential.

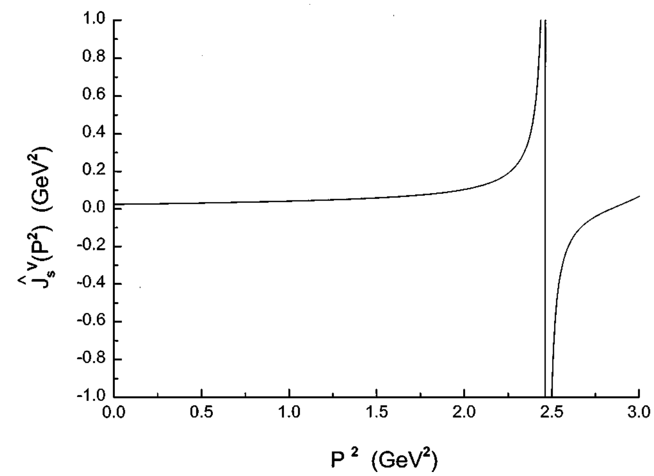


FIG. 4. The figure shows $\hat{J}_s^V(P^2)$ for $m_s = 0.565$ GeV. (Other parameters are those given in the caption to Fig. 3.)

In the case of ideal mixing the expressions for the meson decay constants are simple. We define

$$\langle \mathrm{vac}|J^\mu_{em}|\omega,\lambda\rangle = m_\omega f_\omega \epsilon^\mu_\lambda(\vec{k}), \tag{3.7}$$

for the $\omega$ and its radial excitations. Here $\epsilon^\mu_\lambda(\vec{k})$ is the polarization vector of $\omega$. Thus,

$$f_\omega = \frac{g_{\omega qq}}{\sqrt{2}} \frac{\hat{J}_u^V(m_\omega^2)}{m_\omega}\left(\frac{2}{3} - \frac{1}{3}\right), \tag{3.8}$$

where the last factor arises from the charges of the up and down quarks. We find $g_{\omega qq} = 3.93$ and $\hat{J}_u(m_\omega^2) = 0.040$ GeV$^2$ for the $\omega(782)$. These values yield $f_\omega = 47.4$ MeV, which is close to the experimental value of $f_\omega = 45.9 \pm 0.7$ MeV. (See Table I.) [Note that $\hat{J}_u(m_\omega^2) = (2G_2)^{-1}/2$.]

For the $\phi$ meson, we have

$$f_\phi = g_{\phi qq} \frac{\hat{J}_s(m_\phi^2)}{m_\phi}(1/3). \tag{3.9}$$

In the case of the $\phi(1020)$, we find $g_{\phi qq} = 4.78$ and $\hat{J}_s(m_\phi^2) = (2G_2)^{-1}/2 = 0.040$ GeV$^2$, so that $f_\phi = 62.5$ MeV, which is to be compared to the experimental value of $78 \pm 2$ MeV. We also note the relation of the width $\Gamma(e^+,e^-)$ to the decay constants defined above. For the $\phi$ meson, for example,

$$\Gamma(e^+,e^-) = \frac{4\pi\alpha^2}{3}\frac{f_\phi^2}{m_\phi}. \tag{3.10}$$

### IV. PSEUDOSCALAR MESONS: $\eta$-$\eta'$ MIXING

For the study of pseudoscalar states, we use some of the notation of Ref. [8] where various effective coupling constants were defined. In the presence of the 't Hooft interaction, these coupling constants depend upon the vacuum condensates $\langle \bar{u}u\rangle = \langle \bar{d}d\rangle$ and $\langle \bar{s}s\rangle$. The effective coupling constants are

$$K_{88}^P = 2G_1 + 2Hc_{88}, \tag{4.1}$$

$$K_{00}^P = 2G_1 + 2Hc_{00}, \tag{4.2}$$

$$K_{08}^P = 2Hc_{08}, \tag{4.3}$$

where

TABLE I. Experiment values for the masses and decay constants [10] are compared to our theoretical values. Here $m_u = m_d = 0.364$ GeV, $m_s = 0.565$ GeV, $K = 0.0575$ GeV$^2$, $\Lambda_3 = 0.622$ GeV, $\mu = 0.020$ GeV, and $G_2 = 6.25$ GeV$^{-2}$.

| Meson | Mass (Expt.) (MeV) | Mass (Theory) (MeV) | $g_{\omega qq}$ or $g_{\phi qq}$ | Decay constant $(f_\omega, f_\phi)$ (MeV) Expt. | Theory |
|---|---|---|---|---|---|
| $\omega(782)$ | $781 \pm 0.12$ | 782[a] | 3.93 | $45.9 \pm 0.7$ | 47.4 |
| $\phi(1020)$ | $1019.413 \pm 0.008$ | 1019[a] | 4.78 | $78 \pm 2$ | 62.5 |
| $\omega(1420)$ | $1419 \pm 31$ | 1402 | 1.26 | | 8.4 |
| $\omega(1600)$ | $1649 \pm 24$ | 1650 | 0.861 | | 4.9 |
| $\phi(1680)$ | $1680 \pm 20$ | 1717 | 0.731 | | 5.8 |

[a]Fit by the choice of $G_2$ and $m_s$.

$$c_{00}=-\frac{2}{3}\,(2\langle\bar{u}u\rangle+\langle\bar{s}s\rangle), \tag{4.4}$$

$$c_{88}=\frac{1}{3}\,(4\langle\bar{u}u\rangle-\langle\bar{s}s\rangle), \tag{4.5}$$

and

$$c_{08}=\frac{\sqrt{2}}{3}\,(\langle\bar{u}u\rangle-\langle\bar{s}s\rangle). \tag{4.6}$$

In addition, we define the vacuum polarization function

$$-i\hat{J}_u^P(P^2)=-n_c\int\frac{d^4k}{(2\pi)^4}\,\mathrm{Tr}[iS_u(P/2+k)i\bar{\Gamma}_p(P,k)\times iS_u(-P/2+k)i\gamma_5], \tag{4.7}$$

where the subscript $u$ refers to the up quark. There is a similar definition for $J_s^P(P^2)$. (See Appendix C.) In terms of these functions, we define

$$\hat{J}_{00}^P(P^2)=\frac{2}{3}\,[\hat{J}_u^P(P^2)+\hat{J}_d^P(P^2)+\hat{J}_s^P(P^2)], \tag{4.8}$$

$$\hat{J}_{88}^P(P^2)=\frac{1}{3}\,[\hat{J}_u^P(P^2)+\hat{J}_d^P(P^2)+4\hat{J}_s^P(P^2)], \tag{4.9}$$

and

$$\hat{J}_{08}^P(P^2)=\frac{\sqrt{2}}{3}\,[\hat{J}_u^P(P^2)+\hat{J}_d^P(P^2)-2\hat{J}_s^P(P^2)]. \tag{4.10}$$

With reference to Eqs. (4.1)–(4.3) and to Eqs. (4.8)–(4.10), we define

$$K_P=\begin{pmatrix} K_{88}^P & K_{08}^P \\ K_{08}^P & K_{00}^P \end{pmatrix}, \tag{4.11}$$

and

$$\hat{J}^P(P^2)=\begin{pmatrix} \hat{J}_{88}^P(P^2) & \hat{J}_{08}^P(P^2) \\ \hat{J}_{08}^P(P^2) & \hat{J}_{00}^P(P^2) \end{pmatrix}. \tag{4.12}$$

We also introduce a $T$ matrix and a matrix $D_P$. If we write

$$T_P(P^2)=\begin{pmatrix} A_P(P^2) & B_P(P^2) \\ B_P(P^2) & C_P(P^2) \end{pmatrix}, \tag{4.13}$$

we have

$$A_P(P^2)=\frac{1}{\det D_P(P^2)}\,\{(K_{00}^PK_{88}^P-K_{08}^PK_{08}^P)\hat{J}_{00}^P(P^2)-K_{88}^P\}, \tag{4.14}$$

$$B_P(P^2)=\frac{1}{\det D_P(P^2)}\,\{-(K_{00}^PK_{88}^P-K_{08}^PK_{08}^P)\hat{J}_{08}^P(P^2)-K_{08}^P\}, \tag{4.15}$$

and

$$C_P(P^2)=\frac{1}{\det D_P(P^2)}\,\{(K_{00}^PK_{88}^P-K_{08}^PK_{08}^P)\hat{J}_{88}^P(P^2)-K_{00}^P\}. \tag{4.16}$$

Further, the matrix $D_P(P^2)$ is

$$D_P(P^2)=\begin{pmatrix} D_{11}^P(P^2) & D_{12}^P(P^2) \\ D_{21}^P(P^2) & D_{22}^P(P^2) \end{pmatrix}, \tag{4.17}$$

with

$$D_{11}^P(P^2)=K_{88}^P\hat{J}_{88}^P(P^2)+K_{08}^P\hat{J}_{08}^P(P^2)-1, \tag{4.18}$$

$$D_{12}^P(P^2)=K_{88}^P\hat{J}_{08}^P(P^2)+K_{08}^P\hat{J}_{00}^P(P^2), \tag{4.19}$$

$$D_{21}^P(P^2)=K_{00}^P\hat{J}_{08}^P(P^2)+K_{08}^P\hat{J}_{08}^P(P^2), \tag{4.20}$$

and

$$D_{22}^P(P^2)=K_{00}^P\hat{J}_{00}^P(P^2)+K_{08}^P\hat{J}_{08}^P(P^2)-1. \tag{4.21}$$

A matrix

$$M(\theta_P)=\begin{pmatrix} \cos\theta_P & -\sin\theta_P \\ \sin\theta_P & \cos\theta_P \end{pmatrix} \tag{4.22}$$

may be used to bring the $T$ matrix to diagonal form with diagonal elements $T_1$ and $T_2$. Thus, $M(\theta_P)T(P^2)M^{-1}(\theta_P)=T_{\mathrm{diag}}(P^2)$ with

$$\tan 2\theta_P(P^2)=\frac{2B_P(P^2)}{C_P(P^2)-A_P(P^2)}. \tag{4.23}$$

We have

$$\begin{pmatrix} \eta \\ \eta' \end{pmatrix}=M(\theta_P)\begin{pmatrix} \eta_8 \\ \eta_0 \end{pmatrix} \tag{4.24}$$

with

$$\eta_8=\frac{1}{\sqrt{6}}\,[\bar{u}\gamma_5u+\bar{d}\gamma_5d-2\bar{s}\gamma_5s], \tag{4.25}$$

and

$$\eta_0=\frac{1}{\sqrt{3}}\,[\bar{u}\gamma_5u+\bar{d}\gamma_5d+\bar{s}\gamma_5s]. \tag{4.26}$$

Note that even with $K_{08}=0$, $\theta_P(P^2)$ is not a constant, since $K_{00}^P\neq K_{88}^P$ in this analysis.

In general, bound state energies can be found by determining the singularities of the $T$ matrix. When the $T$ matrix is not a single function, but has a matrix structure, it is necessary to bring it to diagonal form. It is then seen that a particular resonance is found predominately in one eigenvalue. For example, if we have a matrix of dimension 2, we can write $T(P^2)=|e_1\rangle T_1(P^2)\langle e_1|+|e_2\rangle T_2(P^2)\langle e_2|$ where $|e_1\rangle$ and $|e_2\rangle$ are the eigenfunctions at the value of $P^2$. We have $T(P^2)\simeq|e_1\rangle T_1(P^2)\langle e_1|$ if the resonance is predominately in $T_1(P^2)$. The mixing angle is then exhibited by writing $\langle\Phi|T(P^2)|\Phi\rangle=\langle\Phi|e_1\rangle T_1(P^2)\langle e_1|\Phi\rangle$ where

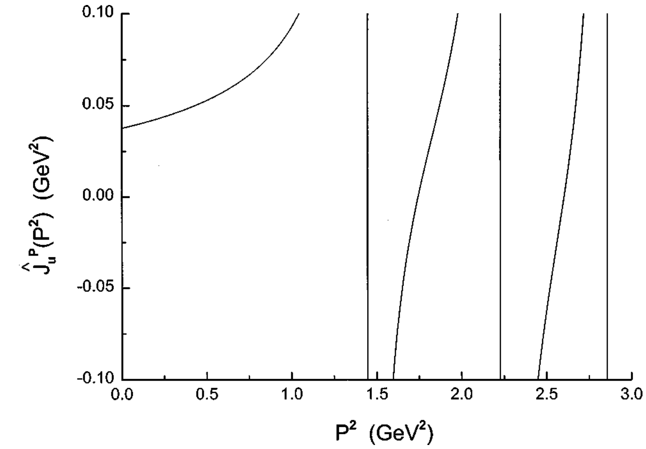


FIG. 5. The function $\hat{J}_u^P(P^2)$ is shown. Here $m_u = 0.364$ GeV, $\Lambda_3 = 0.622$ GeV, and $\mu = 0.020$ GeV. The vertical lines show the energies of bound states of the up (or down) quark in the confining field.

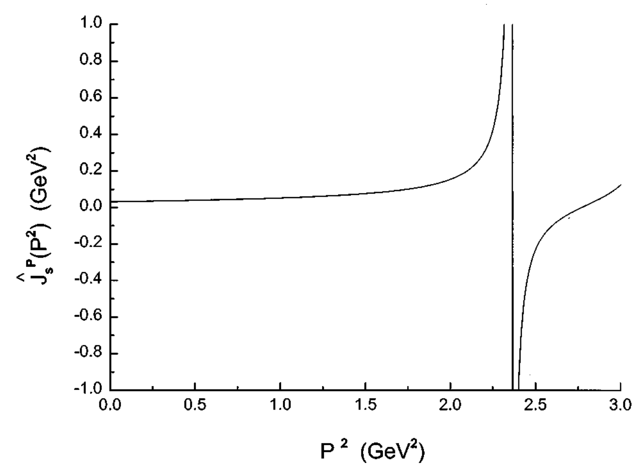


FIG. 6. The function $\hat{J}_s^P(P^2)$ is shown. Here $m_u = 0.364$ GeV, $m_s = 0.565$ GeV, $\Lambda_3 = 0.622$ GeV, $\kappa = 0.0575$ GeV$^2$, and $\mu = 0.020$ GeV.

$$|\Phi\rangle = \begin{pmatrix} \lambda_8 \\ \lambda_0 \end{pmatrix}. \tag{4.27}$$

## V. NUMERICAL RESULTS

Using the procedure outlined in Sec. III, we obtain the results given in Table I for the $\phi$ and $\omega$ mesons. Except for the fact that our prediction for the mass of the $\phi(1680)$ is a bit too large, the results are quite good.

For the calculation of $\eta$ and $\eta'$ mixing we need $J_u^P(P^2)$ and $J_s^P(P^2)$ which are shown in Figs. 5 and 6. For the study of singlet-octet mixing, we put $H = -50.0$ GeV$^{-5}$. We also use the condensate values used by Vogl and Weise [6]. These are $\langle \bar{u}u \rangle = -(0.248\ \text{GeV})^3 = -0.01525$ GeV$^3$ and $\langle \bar{s}s \rangle = -(0.258\ \text{GeV})^3 = -0.01717$ GeV$^3$. We then find that with $G_2 = 6.25$ GeV$^{-2}$, a value used in our study of the $\phi$-$\omega$ system, and $G_1 = 5.69$ GeV$^{-2}$, we obtain 512 MeV for the mass of the $\eta(547)$ and 977 MeV for the mass of the $\eta'(958)$. (See Fig. 7 and Table II.)

In Fig. 8 we show $T_1(P^2)$, the first element of the diagonalized $T$ matrix. We find resonances at $P^2 = 0.262$ GeV$^2$, $P^2 = 0.954$ GeV$^2$, $P^2 = 1.88$ GeV$^2$, and $P^2 = 2.86$ GeV$^2$. The masses are 0.512 GeV [$\eta(547)$], 0.977 GeV [$\eta(958)$], 1.37 GeV, and 1.69 GeV. We show $T_2(P^2)$ in Fig. 9. The resonances are at $P^2 = 0.262$ GeV$^2$, $P^2 = 0.954$ GeV$^2$, and $P^2 = 2.69$ GeV$^2$. The last resonance has a mass value of 1.64 GeV and is not seen in $T_1(P^2)$. Therefore, we have found five states below $P^2 = 3.0$ GeV$^2$. There are the experimentally determined states, the $\eta(1295)$ and the $\eta(1440)$, with energies that do not correspond closely to the theoretical predictions for states of $\bar{q}q$ structure given above. Beyond the $\eta(547)$ and $\eta'(958)$, the theoretical interpretation of the states of higher energy is uncertain. In the data compilation of Ref. [10], it is suggested that the $\eta(1295)$ and $\eta(1440)$ may be non-$\bar{q}q$ configurations. It is also suggested that the $\eta(1440)$ may represent the presence of two states rather than one.

It is worth noting that the state at 1.37 GeV seen in $T_1(P^2)$ is about halfway between the $\eta(1295)$ and $\eta(1440)$. One may speculate that our 1.37 GeV state may mix with a non-$\bar{q}q$ configuration to produce the $\eta(1295)$ and $\eta(1440)$. We are not able to resolve these issues at this time. However, in this work we do provide the predictions of our generalized NJL model for the pure $\bar{q}q$ configurations.

In Table II we present values for $\theta_P(P^2)$ for the five states of the $\eta$-$\eta'$ system found in this work. Inspection of Figs. 8 and 9, shows that the theoretical states at 1.37 GeV and 1.69 GeV are predominantly seen in $T_1$, while the state at 1.64 GeV is seen only in $T_2$. Assigning these states entirely to a single channel allows us to calculate the percentage of $\bar{s}s$ component. From Table II, we see that the state at 1.69 GeV is almost entirely of $\bar{s}s$ character, while the states at 1.37 GeV and 1.64 GeV have only a very small $\bar{s}s$ component. We remark, therefore, that the state 1.69 GeV can be thought of as being in correspondence to the $\phi(1680)$, which is a pure $\bar{s}s$ configuration. Proceeding along these lines, we may think of the $\omega(1420)$ and the theoretical state at 1.37 GeV to be in correspondence. They have little or no $\bar{s}s$ com-

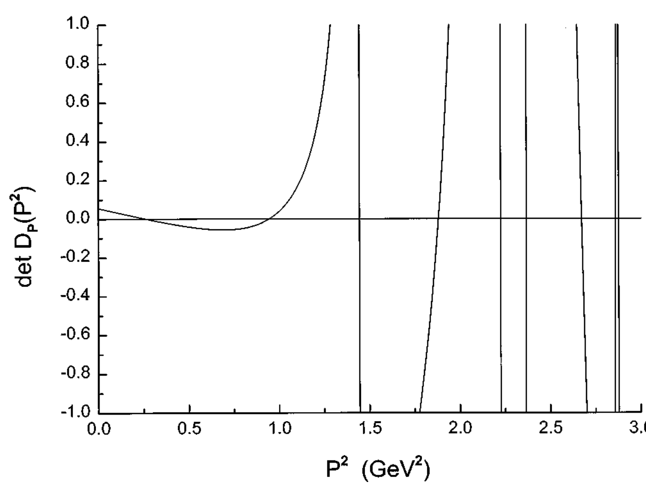


FIG. 7. Values of det $D_P(P^2)$ are shown. The vertical lines represent the singularities of det $D_P(P^2)$ due to the singularities of $\hat{J}_u^P(P^2)$ and $\hat{J}_s^P(P^2)$ seen in Figs. 3 and 4. There are five significant zeros corresponding to states of the coupled $\eta$-$\eta'$ system. (See the captions of Figs. 8 and 9 for the energies of these five states.)

TABLE II. Mass spectrum and mixing angles for states of the $\eta$-$\eta'$ system. For the first three columns $H=-50.0\ \mathrm{GeV}^{-5}$, $G_1=5.69\ \mathrm{GeV}^{-2}$, and only singlet-octet mixing is included. For the last column, pseudoscalar-axialvector mixing is taken into account, $H$ is reduced to $-16.0\ \mathrm{GeV}^{-5}$, and $G_1=6.10\ \mathrm{GeV}^{-2}$ is used. Here $m_u=0.364$ GeV and $m_s=0.565$ GeV. For a resonance in $T_1$ we have $\eta=\cos\theta_p\eta^8-\sin\theta_P\eta^0$, while for a resonance in $T_2$, we have $\eta'=\sin\theta_p\eta^8+\cos\theta_P\eta^0$.

| Mass (theory) (GeV) | $\theta_P(P^2)$ (deg) | Channel | Fraction of $\overline{s}s$ configuration | Mass (GeV) $H=-16.0\ \mathrm{GeV}^{-5}$ |
|---|---|---|---|---|
| 0.512 | −11.5 | $T_1$ | 0.468[a] | 0.531 |
| 0.977 | −36.3 | $T_2$ | 0.897[b] | 0.972 |
| 1.37 | −62.5 | $T_1$ | 0.018[a] | 1.36 |
| 1.64 | 41.5 | $T_2$ | 0.012[b] | 1.63 |
| 1.69 | 35.3 | $T_1$ | 0.998[a] | 1.69 |

[a]Calculated on the assumption that the resonance appears only in $T_1$ (see Figs. 8 and 9).
[b]Calculated on the assumption that the resonance appears entirely in $T_2$ (see Figs. 8 and 9).

ponent and may be classed as radial excitations of $2S$ character.

Our analysis may be extended to include pseudoscalar-axialvector coupling in the $\eta$-$\eta'$ system. The necessary formal developments are given in Ref. [8] and we follow the procedure described there. In that work one makes use of the fact that the $T$ matrix factors at each resonance with a vertex function of the form [8]

$$V(P)=g_\eta i\gamma_5(\cos\hat{\theta}\lambda_8-\sin\hat{\theta}\lambda_0)+\frac{\tilde{g}_\eta}{2m_{us}}\,i\not{P}\gamma_5 \times(\cos\tilde{\theta}\lambda_8-\sin\tilde{\theta}\lambda_0), \tag{5.1}$$

with $m_{us}=[(m_u+2m_s)\cos^2\tilde{\theta}+(2m_u+m_s)\sin^2\tilde{\theta}]/3$. To obtain good values for the $\eta$ and $\eta'$ masses, we find we have to reduce $H=-50.0\ \mathrm{GeV}^{-5}$ to $H=-16.0\ \mathrm{GeV}^{-5}$. That is, the inclusion of pseudoscalar-axialvector coupling leads to the use of a significantly smaller strength for the 't Hooft interaction if we wish to fit the value of $m_\eta$ and $m_{\eta'}$. With $G_1=5.69\ \mathrm{GeV}^{-2}$ and $G_2=6.25\ \mathrm{GeV}^{-2}$ we obtain the results given in Table III.

## VI. DISCUSSION

Our results for singlet-octet mixing with $H=-50.0\ \mathrm{GeV}^{-5}$ were given in Sec. IV. We have recalculated the $\eta$ mass values including pseudoscalar-axialvector mixing and found that reasonable mass values are found when $H$ is reduced to $-16.0\ \mathrm{GeV}^{-5}$. (See Table II.) (A better value for the mass of the $\eta$ is obtained with the smaller value of $H$.) Thus, we see that pseudoscalar-axialvector mixing is important and a complete analysis should be made for that case. Since we were mainly interested in applications of our confinement model, we have not carried out the full program at this time.

Work related to ours has been reported by Takizawa, Nemoto, and Oka [11]. (These authors did not include pseudoscalar-axialvector mixing in their study.) They use the SU(3)-flavor NJL model supplemented with 't Hooft interaction and obtain satisfactory results for the decay rates of the

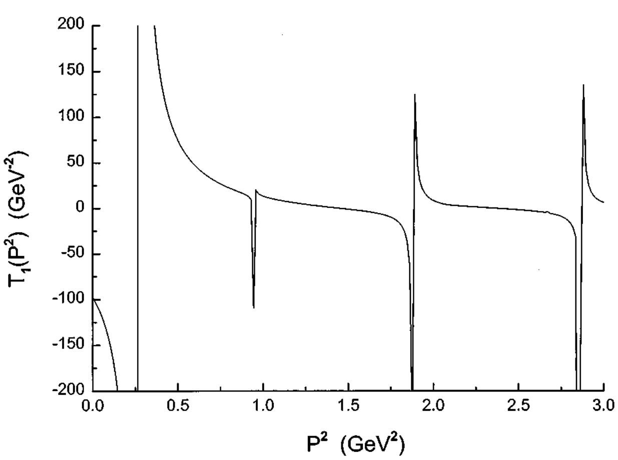


FIG. 8. Values of $T_1(P^2)$ are shown. Resonances are seen at $P^2=0.282\ \mathrm{GeV}^2$ [$\eta(547)$], $P^2=0.945\ \mathrm{GeV}^2$ [$\eta(958)$], $P^2=1.85\ \mathrm{GeV}^2$, and $P^2=2.82\ \mathrm{GeV}^2$, where the bracketed meson designation shows the correspondence with experimental data. The $\eta'$ resonance at $P^2=0.945\ \mathrm{GeV}^2$ has only a relatively small component in $T_1(P^2)$, but is quite strong in $T_2(P^2)$. (See Fig. 9.) The masses of the four states seen here are 0.531 GeV, 0.972 GeV, 1.36 GeV, and 1.69 GeV.

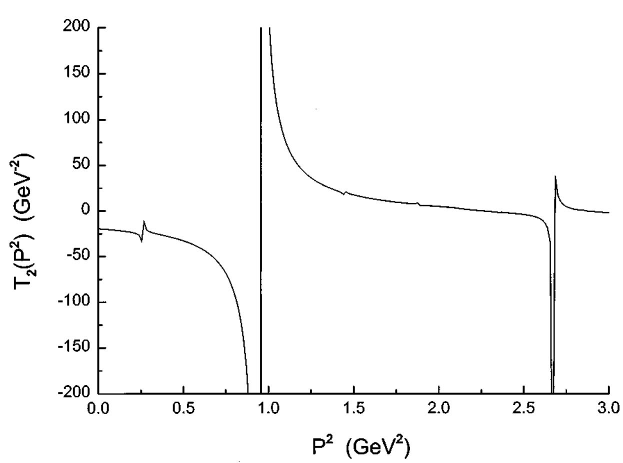


FIG. 9. Values of $T_2(P^2)$ are shown. Resonant behavior is seen at $P^2=0.282\ \mathrm{GeV}^2$ [$\eta(547)$], $P^2=0.945\ \mathrm{GeV}^2$ [$\eta(958)$], and $P^2=2.66\ \mathrm{GeV}^2$. (For the last state the mass is 1.63 GeV.) Note that the $\eta(547)$ has only a small component in $T_2(P^2)$, while the $\eta'(958)$ is quite strong in this component of the $T$ matrix. (See Fig. 8.)

TABLE III. Values of the mixing angles and coupling constants for the vertex of Eq. (5.1). Here $H=-16.0\ \mathrm{GeV}^{-5}$, $G_1=6.10\ \mathrm{GeV}^{-2}$, $G_2=6.25\ \mathrm{GeV}^{-2}$, and $m_{us}=0.433$ GeV.

| Mass (GeV) | $\hat{\theta}(P^2)$ (deg) | $\tilde{\theta}(P^2)$ (deg) | $g_\eta$ | $\tilde{g}_\eta$ |
|---|---|---|---|---|
| 0.531 | −36.7 | −42.9 | 5.50 | 1.90 |
| 0.972 | −135 | −127 | 5.54 | 1.67 |
| 1.36 | −59.6 | 160.3 | 1.19 | 0.074 |
| 1.63 | −135.3 | −121 | 0.380 | 0.365 |
| 1.69 | −52.9 | −56.4 | 0.500 | 0.460 |

$\eta$ to several final states. However, since they did not include a model of confinement, their analysis was limited to the study of the $\eta$. These authors also note that the inclusion of the 't Hooft interaction makes for a $P^2$-dependent mixing angle. [They remark that, since the $\eta$ and $\eta'$ are composites, rather than elementary fields, the term "mixing angle" is a somewhat inappropriate designation for the $P^2$-dependent $\theta_P(P^2)$. We will continue to use that name for $\theta_P(P^2)$ with that reservation in mind.]

A review of work concerning the $\eta$ and $\eta'$ and based upon the solution of coupled Schwinger-Dyson and Bethe-Salpeter equations has been given by Klabucar and Kekez [12]. These authors make use of what is often called the global color model [13]. That work is not unlike the NJL-based approach. It has a more microscopic aspect, since gluons appear in the Schwinger-Dyson equation for the quark self-energy. The infrared (nonperturbative) part of the gluon propagator is parameterized by a Gaussian form of purely phenomenological character. For example, in Ref. [14] we find the gluon propagator

$$G_{\mu\nu}(k)=-\left[g_{\mu\nu}-\frac{k_\mu k_\nu}{k^2}\right]G(k^2), \tag{6.1}$$

with

$$G(k)=G_{\mathrm{UV}}(k^2)+G_{\mathrm{IR}}(k^2). \tag{6.2}$$

Here, $G_{\mathrm{UV}}(k^2)$ represents the known high-momentum behavior and

$$G_{\mathrm{IR}}=\frac{16\pi^2}{3}\,ak^2e^{-\mu k^2} \tag{6.3}$$

is a phenomenological form. Here $a$ and $\mu$ are parameters of the model. It is also necessary to specify five mass parameters for the quarks. One finds a good fit to very many mesonic masses in a model with a limited number of parameters [14]. It is interesting to note that the configuration-space potential obtained from use of Eqs. (6.2)–(6.3) is approximately linear up to about $r=1$ fm. Therefore, we believe that the model of Ref. [14], is not very different from ours in that Lorentz-vector confinement is used.

If we consider only singlet-octet mixing, the use of the 't Hooft interaction in our work solves the problem of getting a large mass for the $\eta_0$. In the discussion of Ref. [14], one finds that an additional mass has to be assigned to the $\eta_0$. That introduces another parameter in the model. Therefore, the treatment of this problem on the basis of the 't Hooft interaction is more satisfactory, since that interaction has its basis in a study of instanton dynamics in QCD [15]. (Of course, the use of the 't Hooft interaction does introduce another parameter, $H$, in our analysis. Both the mass of the $\eta$ and the mass of the $\eta'$ are affected by the 't Hooft interaction to a significant degree [11].)

One may be concerned with the fact that we have used constant values for the constituent quark masses, rather than the momentum-dependent masses that arise when solving the Schwinger-Dyson and Bethe-Salpeter equations [14]. However, it may be seen from Fig. 2 of Ref. [14] that the (Euclidean-space) running mass for the up and down quarks in fairly constant up to about 600 MeV for $\Lambda_{\mathrm{QCD}}\simeq 200$ MeV. Since the cutoff on the vacuum polarization integrals, $\hat{J}(P^2)$, is $\Lambda_3=0.622$ GeV in our calculations, it would appear that our use of constant mass values will not introduce large uncertainties in our results. It also appears that extrapolation of the results given in Fig. 2 of Ref. [14] would lead to fairly constant values of the Minkowski-space mass over a significant range of momentum. Related to this point is the observation that a difference between our simplified model and the work of Ref. [14] is that the calculations of Ref. [14] are carried out in Euclidean space and require an extrapolation into the timelike region. For the running mass, this is done by fitting a fifth-order polynomial to the low-momentum region of the functions describing the momentum-dependent masses. This extrapolation was found to be reliable for all mesonic ground states, but for only a limited number of radial excitations. Results are given in Ref. [14] only for those radial excitations where the method appeared to be reliable: $\pi(2S)$, $\rho(2S)$, $K(2S)$, $J/\psi(2S)$, $Y(2S)$, $Y(3S)$ and a large number of $2S$ states of "open flavor" mesons.

Finally, we note that the inclusion of pseudoscalar-axialvector mixing in addition to singlet-octet mixing changes the physical picture, since we need only a small 't Hooft interaction in that case. That leads to approximate ideal mixing for the $\eta$-$\eta'$ pair. (See Table III.) It is necessary to calculate various decay rates for the $\eta$ and $\eta'$ to see if the results obtained with a small 't Hooft interaction are consistent with experimental data. (See Fig. 10.)

## APPENDIX A: VACUUM POLARIZATION DIAGRAMS

A basic feature of the NJL model are vacuum polarization diagrams of the type shown in Fig. 1. If a quark of a single flavor is considered, we define the tensor

$$-iJ^{\mu\nu}(P)=(-1)n_c\int\frac{d^4k}{(2\pi)^4}\,\mathrm{Tr}[iS(P/2+k)\hat{\gamma}^\mu \times iS(-P/2+k)\hat{\gamma}^\nu], \tag{A1}$$

where $\mathbf{S}(p)=[\not p-m_q+i\epsilon]^{-1}$. Here, $n_c=3$ is the number of colors and

$$\hat{\gamma}^\nu=\gamma^\nu-\frac{\not P P^\nu}{P^2}. \tag{A2}$$

Also, $m_q$ is the constituent mass of the quark. Note that $P_\nu\hat{\gamma}^\nu=0$. Our definition of the vertex $\Gamma^\mu$ also leads to

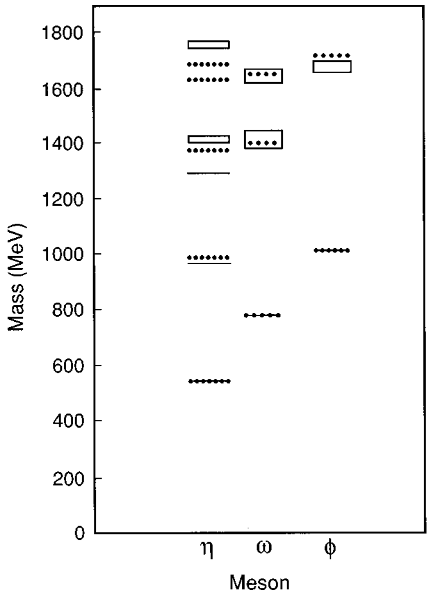


FIG. 10. Theoretical values for the $\eta$, $\eta'$, $\omega$, and $\phi$ masses are shown as dotted lines. The experimental values, with their uncertainties, are shown as solid lines.

$P^\mu\Gamma_\mu=0$, so that $P_\mu J^{\mu\nu}=J^{\mu\nu}P_\nu=0$. (These relations would appear naturally in a fully gauge-invariant calculation, as discussed in Ref. [16].)

Our confinement model leads to the replacement of $J^{\mu\nu}(P^2)$ by $\hat{J}^{\mu\nu}(P^2)$, where

$$-i\hat{J}^{\mu\nu}(P)=(-1)n_c\int\frac{d^4k}{(2\pi)^4}\,\mathrm{Tr}[iS(P/2+k)\Gamma^\mu(P,k)\times iS(-P/2+k)\hat{\gamma}^\nu]. \tag{A3}$$

Here we have replaced $\hat{\gamma}^\mu$ of Eq. (A1) by the confining vertex $\Gamma^\mu(P,k)$. [The calculation of $\Gamma^\mu(P,k)$ is described in the next section.] The evaluation of $\hat{J}_{\mu\nu}(P)$ is made by first carrying out the integral over $k^0$ in the complex $k^0$ plane [17]. To that end, we write

$$S(k)=\frac{m_q}{E(\vec{p})}\left[\frac{\Lambda^{(+)}(\vec{p})}{p^0-E(\vec{p})+i\epsilon}-\frac{\Lambda^{(-)}(-\vec{p})}{p^0+E(\vec{p})-i\epsilon}\right]. \tag{A4}$$

Further, we also need to define

$$\Lambda^{(+)}(\vec{p})=\sum_s u(\vec{p},s)\overline{u}(\vec{p},s), \tag{A5}$$

$$=\frac{\not{p}+m_q}{2m_q}, \tag{A6}$$

$$\Lambda^{(-)}(-\vec{p})=-\sum_s \nu(-\vec{p},-s)\bar{\nu}(-\vec{p},-s), \tag{A7}$$

$$=\frac{\tilde{\not{p}}+m_q}{2m_q}, \tag{A8}$$

with $p^\mu=[E(\vec{p}),\vec{p}]$ and $\tilde{p}^\mu=[-E(\vec{p}),\vec{p}]$. Also

$$\hat{k}^\mu=k^\mu-\frac{(k\cdot P)P^\mu}{P^2} \tag{A9}$$

and

$$\gamma_\perp^\mu(k)=\hat{\gamma}^\mu-\frac{(\hat{\gamma}\cdot\hat{k})\hat{k}^\mu}{\hat{k}^2}. \tag{A10}$$

Note that $P_\mu\gamma_\perp^\mu(k)=\hat{k}_\mu\gamma_\perp^\mu(k)=0$. Some motivation for introducing $\tilde{k}_\mu$ and $\gamma_\perp^\mu(k)$ may be seen by working in the frame where $\vec{P}=0$. There, $\hat{k}^\mu=[0,\vec{k}]$ and $\gamma_\perp^\mu(k)=[0,\vec{\gamma}_\perp(\vec{k})]$, where $\vec{\gamma}_\perp(\vec{k})$ is orthogonal to $\vec{k}$. Thus, $\hat{k}^\mu$ is associated with the longitudinal mode and $\gamma_\perp^\mu(k)$ provides a basis for describing the transverse modes. In terms of these basis vectors, it is useful to define functions $\Gamma_1^{+-}(P,k)$, $\Gamma_2^{+-}(P,k)$, $\Gamma_1^{-+}(P,k)$, and $\Gamma_2^{-+}(P,k)$, by the relations [9]

$$\Lambda^{(+)}(\vec{k})\Gamma^\mu\Lambda^{(-)}(-\vec{k})=\Gamma_1^{+-}\hat{k}^\mu\Lambda^{(+)}(\vec{k})\Lambda^{(-)}(-\vec{k})+\Gamma_2^{+-}\Lambda^{(+)}(\vec{k})\gamma_\perp^\mu(k)\Lambda^{(-)}(-\vec{k}) \tag{A11}$$

and

$$\Lambda^{(-)}(-\vec{k})\Gamma^\mu\Lambda^{(+)}(\vec{k})=\Gamma_1^{-+}\hat{k}^\mu\Lambda^{(-)}(-\vec{k})\Lambda^{(+)}(\vec{k})+\Gamma_2^{-+}\Lambda^{(-)}(-\vec{k})\gamma_\perp^\mu(k)\Lambda^{(+)}(\vec{k}). \tag{A12}$$

Further details of our calculation may be found in Ref. [9]. We define

$$\hat{J}^{\mu\nu}(P)=-\hat{g}^{\mu\nu}(P)\hat{J}(P^2), \tag{A13}$$

where

$$\hat{g}^{\mu\nu}=g^{\mu\nu}=\frac{P^\mu P^\nu}{P^2}. \tag{A14}$$

In Ref. [16] we presented a detailed derivation of our expression for $\hat{J}(P^2)$,

$$\hat{J}(P^2)=-n_c\int\frac{d^3k}{(2\pi)^3}\left[\frac{m_q}{E(\vec{k})}\right]^2\left[\frac{a_1^{+-}\Gamma_1^{+-}+a_2^{+-}\Gamma_2^{+-}}{P^0-2E(\vec{k})}-\frac{a_1^{-+}\Gamma_1^{-+}+a_2^{-+}\Gamma_2^{-+}}{P^0+2E(\vec{k})}\right]. \tag{A15}$$

Here, $a_1^{+-}=-2\vec{k}^2/(3m_q)$, $a_2^{+-}=4E^2(\vec{k})/(3m_q^2)$, $a_1^{-+}=a_1^{+-}$ and $a_2^{-+}=a_2^{+-}$. The integral of Eq. (A15) is divergent and requires a cutoff. We take $|\vec{k}|\leqslant\Lambda_3$ where $\Lambda_3$ is the regulator. In the absence of a confining potential, we have $\Gamma_1^{+-}=\Gamma_1^{-+}=-m_q/\vec{k}^2$ and $\Gamma_2^{+-}=\Gamma_2^{-+}=1$. In that case, we obtain the result of the original NJL model for $\vec{P}=0$,

$$J(P^2)=n_c\int \frac{d^3k}{(2\pi)^3}\frac{1}{2E(\vec{k})}\frac{4E^2(\vec{k})-(4/3)\vec{k}^2}{E^2(\vec{k})-(P^0)^2/4}, \tag{A16}$$

where, again, the cutoff $\Lambda_3$ is used to regulate the integral. For the study of light mesons, $\Lambda_3$ is taken to be about 0.6 to 0.7 GeV. (The corresponding Euclidean-space evaluation of the 4-dimensional integral over $k^\mu$ makes use of a cutoff $\Lambda_E$, that is about 0.9–1.0 GeV.)

When studying the omega meson (with $m_u=m_d$), we define $\hat{J}_\omega(P^2)=2\hat{J}_u(P^2)=2\hat{J}_d(P^2)$.

As in Ref. [9], we calculate the second term of Eq. (A15) by using $\Gamma_1^{-+}=-m_q/\vec{k}^2$ and $\Gamma_2^{-+}=1$. That should be a good approximation, since the second term of Eq. (A15) is already small due to the form of the denominator.

## APPENDIX B: VERTEX FUNCTIONS FOR A CONFINING INTERACTION: VECTOR MESONS

A comprehensive discussion of the equation for the vertex functions was given in Ref. [4] for the case of Lorentz-scalar confinement. We had

$$\Gamma_\mu(P,k)=\hat{\gamma}_\mu+i\int\frac{d^4q}{(2\pi)^4}S(P/2+q)\Gamma_\mu(P,q)\times S(-P/2+q)V^C(|\vec{k}-\vec{q}|), \tag{B1}$$

where $V^C(|\vec{k}-\vec{q}|)$ is the Fourier transform of the confinement potential which was given in Eq. (2.3). Lorentz-vector confinement is described by the following equation for the vertex

$$\Gamma_\mu(P,k)=\hat{\gamma}_\mu-i\int\frac{d^4q}{(2\pi)^4}\gamma^\nu S(P/2+q)\Gamma_\mu(P,q)\times S(-P/2+q)\gamma_\nu V^C(|\vec{k}-\vec{q}|). \tag{B2}$$

The new feature relative to Eq. (B1) is the appearance of a minus sign and a contraction with the Dirac matrix $\gamma^\nu$ in Eq. (B2).

At this point it is useful to define functions $\gamma_1$ and $\gamma_2$. When $\vec{P}=0$, we have [8]

$$\gamma_1(P^0,|\vec{k}|)=-(\vec{k}^2/m_q)\Gamma_1^{+-}(P^0,|\vec{k}|) \tag{B3}$$

and

$$\gamma_2(P^0,|\vec{k}|)=\Gamma_2^{+-}(P^0,|\vec{k}|). \tag{B4}$$

For $|\vec{k}|$ sufficiently large, we can see that $\gamma_1(P^0,|\vec{k}|)\to 1$ and $\gamma_2(P^0,|\vec{k}|)\to 1$ [17]. Further, if we define

$$k_{\rm on}=[(P^0/2)^2-m_q^2]^{1/2}, \tag{B5}$$

we have $\Gamma_1^{+-}(P^0,k_{\rm on})=\Gamma_2^{+-}(P^0,k_{\rm on})=0$. Thus, $\Gamma_1^{+-}(P^0,|\vec{k}|)/[P^0-2E(\vec{k})]$ is finite and we may drop the $i\epsilon$ that would be needed in the denominator in the absence of a confinement model. That feature eliminates the cut that would otherwise appear in $J(P^2)$ for $P^2>(2m_q)^2$. Thus, $\hat{J}(P^2)$ is a real function.

Equations for $\gamma_1(P^0,|\vec{k}|)$ and $\gamma_2(P^0,|\vec{k}|)$ were obtained in Ref. [9] by a technique that involved the calculation of a number of traces of Dirac matrix products. The equations for the case of Lorentz-scalar confinement, with $k=|\vec{k}|$ and $q=|\vec{q}|$, were

$$\gamma_\alpha(P^0,k)=1+\sum_{\alpha'=1,2}\int\frac{dq}{P^0-2E(q)}h_{\alpha\alpha'}(k,q)\gamma_{\alpha'}(P^0,q), \tag{B6}$$

$$h_{11}(k,q)=\frac{kq^3}{2E^2(q)}\left\{(E(k)E(q)+m_q^2)\frac{a_2}{kq}-a_1\right\}, \tag{B7}$$

$$h_{22}(k,q)=\frac{kq^3}{2E(k)E(q)}\left\{(E(k)E(q)+m_q^2)\frac{a_0+a_2}{2kq}-a_1\right\}, \tag{B8}$$

$$h_{12}(k,q)=\frac{[E(q)+E(k)]q^2}{2E(q)}(a_0-a_2), \tag{B9}$$

and

$$h_{21}(k,q)=\frac{[E(k)+E(q)]}{4E(k)E^2(q)}m_q^2q^2(a_0-a_2). \tag{B10}$$

In these equations,

$$a_i(k,q)=-\frac{2\kappa}{\pi}\left(\frac{1}{y^2}A_{i2}+\frac{4\mu^2}{y^3}A_{i3}\right), \tag{B11}$$

where $y=2kq$, $z=(k^2+q^2+\mu^2)/y$ and

$$A_{nm}(z)=\int_{-1}^{1}dt\,\frac{t^n}{(t-z)^m}. \tag{B12}$$

For Lorentz-vector confinement we have, for $\alpha=1,2$,

$$\gamma_\alpha(P^0,k)=1+\sum_{\alpha'=1,2}\int\frac{dq}{P^0-2E(q)}g_{\alpha\alpha'}(k,q)\gamma_{\alpha'}(P^0,q), \tag{B13}$$

with

$$g_{11}(k,q)=\frac{q^2}{E^2(q)}(2qka_1+m_q^2a_2), \tag{B14}$$

$$g_{12}(k,q)=q^2(a_0-a_2), \tag{B15}$$

$$g_{21}(k,q)=\frac{m_q^2q^2}{2E^2(q)}(a_0-a_2), \tag{B16}$$

$$g_{22}(k,q)=\frac{q^3k}{E(k)E(q)}a_1+\frac{q^2}{2}(a_0+a_2). \tag{B17}$$

Note that the equations for $\gamma_1(P^0,k)$ and $\gamma_2(P^0,k)$ do not require a cutoff at high momentum. In numerical calculations, it is usually sufficient to consider momenta for which $k$ and $q$ are less than 4.0 GeV. It is also worth recalling that, when calculating the vacuum polarization diagrams, there is a cutoff of $\Lambda_3$ on the magnitude of $\vec{k}$. Therefore, only values of $\gamma_1(P^0,|\vec{k}|)$ and $\gamma_2(P^0,|\vec{k}|)$ are needed for $|\vec{k}|\leqslant\Lambda_3$ in the calculation of the various $\hat{J}(P^2)$. It is also worth noting that $a_0(k,q)$, $a_1(k,q)$, and $a_2(k,q)$ are quite large when $k=q$. [That behavior reflects the infrared singularity of $V^C(|\vec{k}-\vec{q}|)$.] Because of that behavior, the values obtained for $\gamma_1(P^0,|\vec{k}|)$ and $\gamma_2(P^0,|\vec{k}|)$ for $|\hat{k}|<2.0$ GeV are insensitive to any high-momentum cutoff of value greater than 2.0 GeV, that we use in solving Eq. (B6) or Eq. (B13).

## APPENDIX C: VERTEX FUNCTIONS FOR A CONFINING INTERACTION: PSEUDOSCALAR MESONS

In this appendix we discuss the vertex operator of the confining field for the case of pseudoscalar mesons. With reference to Fig. 1, we may write

$$\overline{\Gamma}_p(P,k)=\gamma_5-i\int\frac{d^4k'}{(2\pi)^4}[\gamma^\mu S(P/2+k')\overline{\Gamma}_p(P,k')\times S(-P/2+k')\gamma_\mu V^C(k-k')]. \tag{C1}$$

Here $S(p)=[\not{p}-m_u+i\epsilon]^{-1}$, if we consider an up quark and an up antiquark at the vertex. We define $\Gamma_p^{+-}$ and $\Gamma_p^{-+}$ such that

$$\Lambda^{(+)}(\vec{k})\overline{\Gamma}_p(P,k)\Lambda^{(-)}(-\vec{k})=\Gamma_p^{+-}(P,k)\Lambda^{(+)}(\vec{k})\gamma_5\Lambda^{(-)}(-\vec{k}), \tag{C2}$$

and

$$\Lambda^{(-)}(-\vec{k})\overline{\Gamma}_p(P,k)\Lambda^{(+)}(\vec{k})=\Gamma_p^{-+}(P,k)\Lambda^{(-)}(-\vec{k})\gamma_5\Lambda^{(+)}(\vec{k}). \tag{C3}$$

Recall that $\Lambda^{(+)}(\vec{k})$ and $\Lambda^{(-)}(-\vec{k})$ were defined in Eqs. (A5) and (A7). The analysis proceeds by multiplying Eq. (C1) from the left by $\gamma_5\Lambda^{(+)}(\vec{k})$ and from the right by $\Lambda^{(-)}(-\vec{k})$ and using Eq. (A4) for the two quark propagators. At that point, we form the trace of the equation. If we divide the equation by $\mathrm{Tr}[\gamma_5\Lambda^{(+)}(\vec{k})\gamma_5\Lambda^{(-)}(-\vec{k})]$, we obtain an equation for $\Gamma_p^{+-}(P,k)$, which involves both $\Gamma_p^{+-}(P,k')$ and $\Gamma_p^{-+}(P,k')$ on the right-hand side. We neglect the coupling of $\Gamma_p^{+-}(P,k)$ to $\Gamma_p^{-+}(P,k)$. In that approximation $\Gamma_p^{+-}(P,k)$ satisfies an uncoupled equation, as does $\Gamma_p^{-+}(P,k)$. The neglect of the coupling term is equivalent to the neglect of ''$Z$ graphs,'' or pair-current effects. Such effects are quite large in the case of Lorentz-vector confinement and they create major problems, if one attempts to solve the coupled equations. Since the probability of the confining potential to excite pair currents is unknown, it is not unreasonable to neglect such effects in the Lorentz-vector confinement model.

Our procedure then requires that we complete the $k_0'$ integral in the lower half of the complex $k_0'$ plane, picking up only the pole where the quark goes on its positive mass shell [17]. The equation, in the frame where $\vec{P}=0$, is found to be

$$\Gamma_p^{+-}(P^0,|\vec{k}|)=1-\int\frac{d^3k'}{(2\pi)^3}\frac{V^C(\vec{k}-\vec{k}')}{P^0-2E(\vec{k}')}\times\frac{m^2-2E(\vec{k})E(\vec{k}')}{E(\vec{k})E(\vec{k}')}\Gamma_p^{+-}(P^0,|\vec{k}'|) \tag{C4}$$

for the equal mass case.

To obtain the corresponding equation for $\Gamma_p^{-+}(P^0,|\vec{k}|)$, we multiply Eq. (C1) by $\gamma_5\Lambda^{(-)}(-\vec{k})$ from the left and $\Lambda^{(+)}(\vec{k})$ from the right and then take the trace of the equation. In this case, we divide the equation by $\mathrm{Tr}[\gamma_5\Lambda^{(-)}(-\vec{k})\gamma_5\Lambda^{(+)}(\vec{k})]$ to obtain an equation for $\Gamma_p^{-+}(P^0,|\vec{k}|)$. The integral over $k_0'$ is completed in the lower-half $k_0'$ plane, where we pick up only the pole that has the antiquark on its *negative* mass shell. The resulting (uncoupled) equation for $\Gamma_p^{-+}(P^0,|\vec{k}|)$ is

$$\Gamma_p^{-+}(P^0,|\vec{k}|)=1+\int\frac{d^3k'}{(2\pi)^3}\frac{V^C(\vec{k}-\vec{k}')}{P^0+2E(\vec{k}')}\times\frac{m^2-2E(\vec{k})E(\vec{k}')}{E(\vec{k})E(\vec{k}')}\Gamma_p^{-+}(P^0,|\vec{k}'|). \tag{C5}$$

For completeness, we record the coupled equations obtained when we pick up both poles in the lower complex $k_0'$ plane. These have the quark going on its *positive* mass shell and the antiquark on its *negative* mass shell. We find

$$\begin{bmatrix}\Gamma_p^{+-}(P^0,|\vec{k}|)\\ \Gamma_p^{-+}(P^0,|\vec{k}|)\end{bmatrix}=\begin{bmatrix}1\\1\end{bmatrix}-\int\frac{d^3k'}{(2\pi)^3}\frac{V^C(\vec{k},\vec{k}')}{E(\vec{k})E(\vec{k}')}\begin{bmatrix}\dfrac{m^2-2E(\vec{k})E(\vec{k}')}{P^0-2E(\vec{k}')} & \dfrac{m^2+2E(\vec{k})E(\vec{k}')}{P^0+2E(\vec{k}')}\\ -\dfrac{m^2+2E(\vec{k})E(\vec{k}')}{P^0-2E(\vec{k}')} & -\dfrac{m^2-2E(\vec{k})E(\vec{k}')}{P^0+2E(\vec{k}')}\end{bmatrix}\begin{bmatrix}\Gamma_p^{+-}(P^0,|\vec{k}'|)\\ \Gamma_p^{-+}(P^0,|\vec{k}'|)\end{bmatrix}. \tag{C6}$$

One may compare the matrix element that couples $\Gamma_p^{+-}$ to $\Gamma_p^{-+}$ with the element that couples $\Gamma_p^{+-}$ to itself. [See Eq. (C6).] In this manner, one can see the very large amplitude for exciting ''pair currents'' (or $Z$-graphs) in the case of Lorentz-vector confinement. That is, $m^2+E(\vec{k})E(\vec{k}')\gg m^2-E(\vec{k})E(\vec{k}')$, making the off-diagonal term quite important.

[1] C. M. Shakin and Wei-Dong Sun, Phys. Rev. D **55**, 2874 (1997).

[2] L. S. Celenza, Xiang-Dong Li, and C. M. Shakin, Phys. Rev. C **55**, 1492 (1997).

[3] L. S. Celenza, Xiang-Dong Li, and C. M. Shakin, Phys. Rev. C **56**, 3326 (1997).

[4] L. S. Celenza, C. M. Shakin, Wei-Dong Sun, J. Szweda, and Xiquan Zhu, Phys. Rev. D **51**, 3638 (1995).

[5] L. S. Celenza, Bo Huang, and C. M. Shakin, Brooklyn College Report No. BCCNT 97/091/266 (1997) (unpublished).

[6] For reviews of the NJL model and the role of the ’t Hooft interaction, see U. Vogl and W. Weise, Prog. Part. Nucl. Phys. **27**, 195 (1991); S. P. Klevansky, Rev. Mod. Phys. **64**, 649 (1992).

[7] The NJL model, supplemented by the ’t Hooft interaction, was studied by V. Bernard, R. L. Jaffe, and U-G. Meissner, Nucl. Phys. **B308**, 753 (1988).

[8] S. Klint, M. Lutz, U. Vogl, and W. Weise, Nucl. Phys. **A516**, 429 (1990).

[9] L. S. Celenza, C. M. Shakin, Wei-Dong Sun, J. Szweda, and Xiquan Zhu, Ann. Phys. (N.Y.) **241**, 1 (1995).

[10] R. M. Barnett *et al.*, Particle Data Group, Phys. Rev. D **54**, 1 (1996).

[11] M. Takizawa, Y. Nemoto, and M. Oka, Phys. Rev. D **55**, 4083 (1997).

[12] D. Klabucar and D. Kekez, Zagreb Univ. Report No. ZTF-97/R01 (1997); LANL archive: hep-ph/9710206.

[13] C. D. Robert and A. G. Williams, Prog. Part. Nucl. Phys. **33**, 477 (1994).

[14] P. Jain and H. Munczek, Phys. Rev. D **48**, 5403 (1993).

[15] G. ’t Hooft, Phys. Rev. D **14**, 3432 (1976); Phys. Rep. **142**, 357 (1986).

[16] C. M. Shakin and Wei-Dong Sun, Phys. Rev. C **54**, 1414 (1996).

[17] Our evaluation of 4-dimensional integrals is related to the procedures introduced by F. Gross and J. Milana, Phys. Rev. D **43**, 2401 (1991); **45**, 969 (1992).